

Evaluation of a high-resolution regional climate simulation over Greenland

3

FILIP LEFEBRE^{1,2} (*), XAVIER FETTWEIS¹, HUBERT GALLEE³, JEAN-PASCAL VAN YPERSELE¹,
PHILIPPE MARBAIX¹, WOUTER GREUELL⁴, PIERLUIGI CALANCA⁵

6

¹*Institut d'Astronomie et de Géophysique G. Lemaître, Université catholique de Louvain, Louvain-la-Neuve, Belgium*

9 ²*Integral Environmental Studies, Vito (Flemish Institute for Technological Research), Mol, Belgium*

³*Laboratoire de Glaciologie et de Géophysique de l'environnement, Grenoble, France*

12 ⁴*Institute for Marine and Atmospheric Research, Utrecht University, Utrecht, The Netherlands*

15 ⁵*Swiss Federal Research Station for Agroecology and Agriculture, Zurich, Switzerland*

18 (*) Corresponding author address: *Integral Environmental Studies, Vito (Flemish Institute for Technological Research), Boeretang 200, B-2400 Mol, Belgium. Tel: + 32 14 33 68 47, Email: Filip.Lefebre@vito.be*

21 Abstract

A simulation of the 1991 summer has been performed over south Greenland with a coupled

atmosphere-snow regional climate model forced by the ECMWF re-analysis. The simulation is
24 evaluated with in-situ coastal and ice sheet atmospheric and glaciological observations. Modelled
air temperature, specific humidity, wind speed and radiative fluxes are in good agreement with the
available observations although uncertainties in the radiative transfer scheme need further
27 investigation to improve the model performance.

In the sub-surface snow-ice model, surface albedo is calculated from the simulated snow grain
shape and size, snow depth, meltwater accumulation, cloudiness and ice albedo. The use of the
30 snow metamorphism processes allows a realistic modelling of the temporal variations in the surface
albedo during both melting periods and accumulation events. Concerning the surface albedo, the
main finding is that an accurate albedo simulation during the melting season strongly depends on a
33 proper initialization of the surface conditions which mainly results from winter accumulation
processes. Furthermore, in a sensitivity experiment with a constant 0.8 albedo over the whole ice
sheet, the average amount of melt decreased by more than 60% which highlights the importance of
36 a correctly simulated surface albedo.

The use of this coupled atmosphere-snow regional climate model opens new perspectives in the
study of the Greenland surface mass balance due to the represented feedback between the surface
39 climate and the surface albedo which is the most sensitive parameter in energy-balance based
ablation calculations.

42

45

48

51 1. Introduction

One of the unknowns of the projected global warming due to anthropogenic forcing is the expected mean sea-level rise. The contribution of each individual 54 component, i.e., the ocean's thermal expansion as well as the mass budgets of Antarctica, Greenland and the continental small ice caps and glaciers, must be known (Houghton et al., 2001).

57

Experimental campaigns such as EGIG 1959 and 1967 (Ambach, 1988), ETH-Camp (Ohmura et al., 1992), GIMEX (Oerlemans and Vugts, 1993), KABEG 60 (Heinemann, 1999) and PARCA (Thomas et al., 2001) give local instantaneous information of the surface mass balance but it is hazardous to estimate the total Greenland surface mass balance from these measurements because of their limited 63 spatial and/or temporal resolution.

In contrast with these measurements, numerical models offer the possibility to 66 evaluate past, present and future changes in the Greenland mass balance. Numerical models also allow the separation and quantification of each individual process contributing to the ice sheet's mass balance.

69

Van de Wal and Oerlemans (1994) were the first to calculate the Greenland surface mass balance by means of an energy balance model but made use of 72 simple parameterizations for the incoming short and longwave radiation fluxes. Also the turbulent energy fluxes were based on simple linear relationships and no distinction between the sensible and latent heat flux was made.

75

Global circulation models (GCMs) also explicitly calculate the surface energy balance and are suited for climate change experiments. However, their major 78 weakness is their rather coarse horizontal resolution. They are unable to represent for example the Greenland ablation zone which ranges from a few kilometers in the south-east to 100 km at its largest in west-Greenland. Also the ice sheet 81 topography is not exactly represented and leads to important errors in the amount of cloudiness, precipitation and ablation. Ohmura et al. (1996) showed the high sensitivity to horizontal resolution for the simulated precipitation field. 84 Furthermore, Hanna and Valdes (2001) analyzed in detail the ECMWF (European Centre for Medium-Range Weather Forecasts) ERA-15 re-analysis surface climate

data for the period 1979 to 1998 and found that surface albedo and cloud errors
87 need to be rectified if the analysis are used effectively to drive energy balance
models for Greenland ablation calculations.

Another problem is that most GCMs do not include physically based surface
90 albedo parameterizations nor they include ice sheet specific processes such as
refreezing of meltwater which is of major importance in the Greenland higher
93 ablation and percolation zone (Pfeffer et al., 1991). It is of capital importance to
correctly simulate the surface albedo since a small albedo error may induce
important errors in the simulated surface net radiation balance which is the major
96 source of energy to heat and melt snow and ice. Nolin and Stroeve (1997) showed
that even in areas that experience little or no melt, important surface albedo
decreases of 10-20 % are common. These reductions are found to be related to
slow increases of snow grain size.

99

A way to refine and to correct GCM predictions of the Greenland surface mass
balance is to nest a regional climate model (RCM) within GCM generated
102 atmospheric fields. The RCM can be run at a higher resolution, thereby
representing more correctly the topography of the steep Greenland ice sheet
margins which improves the simulated atmospheric fields (Georgi et al., 1999)
105 that force the surface mass balance.

Cassano et al. (2001) presented an evaluation of an annual atmospheric
108 simulation over Greenland with the Polar MM5 model. It should be stressed that
their simulation was compiled from a series of short duration (48 hour), forecast
mode, simulations. From these 48 hour simulations, only the last 24 hours are
111 used. In the Polar MM5, the Greenland ice sheet surface is represented by a
diffusive multi-layer surface model with fixed surface properties. In particular the
use of a fixed surface albedo (0.80) can lead to large errors in the simulated net
114 radiation budget over melting surfaces during the summer .

In this paper, we will present an evaluation of a coupled model run in which a
117 high-resolution (20 km) atmospheric regional climate model is coupled with a
physically based snow-ice model. Specific surface processes such as melting,
percolation and refreezing of meltwater as well as the snow grain metamorphism
120 processes and the closely related snow albedo variations are taken into account.
The coupled regional climate model (RCM) will be applied over south Greenland

123 during the 1991 ablation season. It is nested into the ECMWF ERA-15 re-analysis
123 with a single initialisation procedure at the start of the simulation. In a first
attempt, we will focus on the summer season and the accuracy of the surface
125 albedo simulation. The use of re-analyzed forcing fields instead of present climate
126 GCM output minimizes the errors that could be due to wrong input data. It also
enables us to compare the model output with in-situ observations. This work is
129 part of a long-term research project to better estimate the Greenland climate and
surface mass balance (Gallée et al., 1995; Gallée and Duynkerke, 1997; Lefebre,
2003). In the next section, a brief description of the coupled atmosphere-snow
132 RCM is given. Afterwards, the simulation is described and evaluated through
comparison with near-surface atmospheric and mass balance measurements. In
particular, the simulated surface albedo will be compared with observations from
3 locations on the ice sheet. The reference experiment will also be compared with
135 a sensitivity experiment in which the surface albedo has been kept constant at 0.8
over the ice sheet.

138 **2. Coupled atmosphere-snow regional climate model**

2.1. General description

141 The coupled atmosphere-snow regional climate model used is MAR (Modèle
Atmosphérique Régional). The atmospheric part of MAR is fully described in
Gallée and Schayes (1994) and Gallée (1995). MAR is a hydrostatic primitive
144 equation model in which the vertical coordinate is the normalized pressure

$$\sigma = \frac{p - p_t}{p_s - p_t}$$

147 p , p_t and p_s being the pressure, the constant model top pressure and the surface
pressure, respectively. MAR was originally developed for process studies in the
polar regions but is now besides Antarctica (Naithani et al., 2002) also applied
over Europe for nested climatic studies (Marbaix, 2000; Brasseur et al., 2002).
150 The lateral boundary nudging treatment consists of a buffer zone (width of 5
points) involving "Newtonian" and "diffusive" relaxation terms. Lateral boundary
conditions are updated each 6 hours and a linear interpolation is made in between
153 (Davies, 1983; Marbaix et al., 2003).

156 Sea surface temperatures are prescribed from ECMWF re-analysis. Sea ice is not
modelled explicitly but its distribution is deduced from ECMWF sea surface
temperatures. Inside the ECMWF re-analysis system, satellite observations are
used to define the actual sea-ice distribution (Nomura, 1995). Open water and sea
ice have an albedo of 0.07 and 0.55, respectively. A band of tundra points borders
159 the inland ice sheet. In case of a snow-free tundra surface, the force-restore surface
model of Deardorff (1978) with a soil thermal conductivity of $0.65 \text{ W m}^{-1} \text{ K}^{-1}$ and
an albedo of 0.20 is used to predict the tundra surface temperature. When snow
162 covers the tundra soil, the snow model is used (see below) .

2.2. Snow and ice model

165 The snow model is described in details in Gallée and Duynkerke (1997) and
Gallée et al. (2001). It is validated for a site on the Greenland ice sheet (ETH-
Camp, west Greenland, 1150 m a.s.l.) in Lefebre et al. (2003).

168 In the multi-layered thermodynamic one-dimensional snow model, snow
metamorphism processes are represented by the CROCUS snow metamorphism
laws (Brun et al., 1992). The latter allow, in combination with the detailed
171 meltwater budget representation, to represent the evolution of the snow grain
characteristics (shape and size) and its albedo. Afterwards, the surface albedo is
calculated from (1) the snow albedo, (2) the depth of the snow pack upon the ice
174 or the tundra, (3) the accumulated meltwater (over the ice sheet only) and (4) the
albedo of the underlying ice or tundra.

177 During off-line (forced with observations) simulations at ETH-Camp (west
Greenland), the simulated surface albedo and the simulated surface mass balance
were found to be in good agreement with the observations (Lefebre et al., 2003).

180

In the present article, the same snow model configuration as the one used for the
validation is used with two modifications. The first change deals with the
183 influence of atmospheric cloudiness on the surface albedo. Clouds tend to increase
the proportion of the visible part of the solar radiation spectrum, modifying the
incident solar radiation spectrum. This leads to a small increase of about 0.05 in
186 the broadband surface albedo (Key et al., 2001). The coupling between the
atmospheric part of MAR and its snow model uses a fixed solar radiation
spectrum with the simulated broadband solar incident radiation flux. Therefore an
189 additional term in the surface albedo calculation has been added as in Greuell and
Konzelmann (1994) to account for the small increase in surface albedo (up to
0.05) due to clouds.

192

Secondly, compared to the validated version, the density and grain size and shape
for fresh snow are not calculated with the original CROCUS fresh snowfall
195 parameters (dendricity, sphericity and density). In Lefebre et al. (2003), the
original CROCUS fresh snow fall parameters proved to be adequate for ETH-
Camp summer snowfalls. This is due to the location of the site, which is rather
198 close (40 km) to the ice sheet margin, and the occurrence of abundant surface
melt. The latter rapidly transforms freshly-fallen dendritic snow grains into round
snow grains. In the present simulations, the fresh snow parameters ought to be
201 valid not only in the Greenland ablation zone but also for the rest of the Greenland
ice sheet which also includes the ice sheet dry snow zone where no melt occurs.

Therefore, fresh snow is characterized by a snow density of 300 kg m^{-3} and by

204 round, 0.3 mm large spherical snow grains in agreement with surface snow
observations in the dry snow zone (Morris et al., 1997).

207 **2.3. Model setup**

210 The simulation starts the first of May 1991 and lasts until the end of August, i.e.
123 days which corresponds with the major melting period over the Greenland ice
sheet. Mass balance observations at ETH-Camp during the 1991 field season
revealed that the melting season stopped around mid-August.

213 **Figure 1**

216 Figure 1: The prescribed distribution of MAR mass balance zones on the Greenland ice sheet and
the major locations referred to in the text. From black to light grey over the ice sheet: ice sheet
ablation zone, percolation zone and dry snow zone. The model ablation zone delineation is
specified and taken from Reeh (1991). (Right) MAR surface height (isolines) and the difference
(shades of grey) between MAR and ECMWF model surface height.

219 The integration domain encompasses the southern part of Greenland and its
neighbouring waters (Figure 1). MAR fine-grid topography and soil type for
222 Greenland are taken from the Eckholm (1996) Greenland topography and land
masks. The size of the domain is 2000 km by 2000 km with a high horizontal
resolution of 20 km in order to represent the ice sheet ablation zone and the
225 succession of the different mass balance zones. Denby (2001) examined the
sensitivity of turbulent fluxes and katabatic wind speed maximums to the
horizontal resolution. A resolution of 20 km proved to be a good compromise.
228 Wind speed maxima only slightly increased at 10 km resolution. Therefore, a
resolution of 20km enables a correct representation of the katabatic winds and
henceforth of the turbulent heat fluxes due to the mixing of warmer air from above
231 with the cold air in the vicinity of the ice sheet surface. Although a higher
resolution would still be recommendable for some very steep locations (for
example in east Greenland), previous regional atmospheric simulations with
234 complete 3-dimensional models (e.g. Cassano et al. 2001; Bromwich et al. 2001b)
never used resolutions finer than 40 km. Computing time is still a limiting factor
in regional climatic simulations.

237 Strong vertical gradients of wind speed and temperature are found close to the

surface of the Greenland ice sheet. Therefore the lowest atmospheric model level
 240 has been put at 2 m above the surface. The next 4 levels are situated at 4, 8, 16,
 and 32 m above the surface, respectively. The model has been initialized once.
 The lateral boundaries are updated every 6 hours with the ECMWF ERA-15 re-
 243 analysis for temperature, specific humidity, wind components and surface
 pressure. Linear interpolation in time is made in between.

246 2.4. Initialization

MAR atmospheric wind components, air temperature and specific humidity as
 well as the surface temperatures and deep-soil tundra temperatures are initialized
 249 from the ECMWF ERA-15 re-analysis. Ideally, we should spin-up the snow
 model separately during a long-term period in order to obtain equilibrated snow
 and ice initial temperature and density fields. For our simulations, we have in a
 252 first attempt, prescribed these initial fields. In particular over the ice sheet, the
 snow and ice initial temperatures are initialized by linear interpolation between
 the ECMWF ERA-15 surface temperature and the climatological deep snow and
 255 ice temperature (T_{ann}). The latter was taken from Reeh (1991) who derived a
 parameterization based on long-term ice sheet temperature records for the 1951-
 1961 period. This parameterization, or with slightly different parameters, is also
 258 used in thermodynamic ice sheet models of the Greenland ice sheet as an
 approximation of the annual average surface temperature (see e.g. Huybrechts et
 al. (1991); Ritz et al. (1997)):

$$261 \quad T_{ann}(\text{in } ^\circ\text{C}) = 48.38 - 0.007924 * E - 0.7512 * L \quad (1)$$

with E the surface elevation (m) and L the latitude ($^\circ\text{N}$).

264 The dry snow zone has been delineated as the area with an annual mean
 temperature of less than -25°C (Benson, 1962). The model ablation zone
 delineation is taken from Reeh (1991). In the model ablation zone, the 1990-1991
 267 winter precipitated snow from Bromwich et al. (2001a) is laid on top of a 20 m
 thick prescribed ice pack. By lack of reliable data, we neglect the impact of snow
 drift, evaporation and sublimation. This can eventually lead to an overestimation
 270 of more than 10 % of the snow pack height according Box and Steffen (2001). A
 typical surface snow density of 300 kg m^{-3} has been chosen (Morris et al., 1997).
 In the area between the ablation zone and the dry snow zone (denoted percolation

273 zone) the snow density has been put equal to 500 kg m^{-3} for the lowest 20 m of the
 274 snow pack. On top of it, as in the ablation zone, the Bromwich et al. (2001a)
 275 1990-1991 winter snow fall has been added with a density of 300 kg m^{-3} . In the
 276 dry snow zone, the snow density between the bottom of the snow model at 20 m
 277 depth and the surface snow has been calculated with the empirical density-depth
 278 relation from Schytt (1958):

$$\rho = \rho_i - (\rho_i - \rho_s) * \exp(-C * z) \quad (2)$$

279 where ρ is density at depth z , ρ_i the density of ice (920 kg m^{-3}), ρ_s the density of
 280 surface snow (300 kg m^{-3}), and C is a constant which has been set to $1.9/z_t$ where
 281 z_t is the depth of the firn-ice transition. z_t varies with accumulation rate and surface
 282 climate, and has been put to 70 m, a typical value for Greenland (Paterson, 1994).

283 Lastly, the tundra area has also been covered with the winter 1990-1991 snow
 284 pack since the start of the simulation takes place on the first of May 1991. Table 1
 285 and Figure 1 summarize the details of the snow and ice initial state.

Table 1: Snow-ice model initial state characteristics.

Table 1

286

3. Evaluation of the model results

291 Model grid point results are instantaneous values averaged for the whole grid cell
area. Comparing those values with local observations must be done carefully. The
294 model grid cell closest to the observation site doesn't necessarily have the same
elevation as the observation site. Moreover, sub-grid topography roughness and
local surface variability (surface albedo, surface emissivity and soil heat capacity)
can locally influence the air motion and thermodynamic air characteristics. Higher
297 up the ice sheet, in the dry snow zone, these effects are likely less important since
the surface is more homogeneous and flat. However, in the lower ablation zone
and in the tundra area these effects may be very important. For example,
300 measurements at Kangerlussuaq (67.01°N and 50.70°W) in the tundra area on
west Greenland are influenced by the local conditions since the weather station is
303 situated near the local airport where the surface is covered by asphalt. Table 2
gives an overview of the locations used in the comparison. Data from one coastal
weather station operated by the Danish Meteorological Institute and from four on-
ice sites have been used. One of the ice sheet stations is situated in the dry snow
306 area (AWS-Klinck), two others are located close to the long-term equilibrium line
(ETH-Camp and GIMEX-M9), the last one (GIMEX-M6) is in the ablation zone.

309 Table 2: Geographical positions and elevations of the locations used in the comparison.

Table 2

312 3.1. Model evaluation at ETH-Camp

ETH-Camp is located some 40 km far from the ice sheet margin, close to the long-
315 term equilibrium line. In the model, it is located in a grid cell inside the ice sheet
ablation zone neighbouring the equilibrium line altitude (ELA). A description of
the 1991 intensive measurement campaign at ETH-Camp is given in Ohmura et al.
(1992). In this section we will compare in detail MAR modelled and observed
318 variables at ETH-Camp for the period between May 9 and August 30 in 1991 (see
Figure 2 and Table 3). This is done in order to explain some of the strong points
and deficiencies related to the coupling of the atmospheric model with the snow
321 model. Also the ERA-15 fields interpolated on the MAR grid have been added in

the comparison. ERA-15 fields are linearly interpolated from the 'reduced' Gaussian grid which was used to construct the ERA-15 re-analysis. At 70 deg
 324 North, the ERA-15 west-east resolution is 2.8125 degrees which corresponds to a horizontal resolution of about 106 km. This coarse resolution makes comparisons with point observations difficult. Interpolated ERA-15 values close to the ice sheet
 327 margin will be influenced by the presence of the tundra area.

Figure 2

330 Figure 2: Comparison between observed (dotted), MAR (solid) and ECMWF (dashed) modelled air temperature, relative humidity, wind speed, wind direction and surface pressure (daily average values) at ETH-Camp during the whole simulation.

333 During the whole period, MAR simulated surface boundary layer (SBL) temperatures are in close agreement with the observations. On the contrary, the
 336 ERA-15 SBL temperatures are overestimated during the month of July. Furthermore the ERA-15 humidity and wind speed in the SBL are underestimated during that period, while the same variables in MAR are in closer agreement with
 339 the observations (see also Table 3).

342 These deficiencies are probably caused by a coarse representation of the ECMWF planetary boundary layer. First the larger height of the first vertical layer in the
 345 ECMWF model (roughly 40 m) compared to that of the MAR model (roughly 2 m) induces errors in the representation of the katabatic vertical structure. In fact, the vertical profile of the persistent katabatic wind speed exhibits a low level wind speed maximum that is not resolved in the ECMWF model. The katabatic winds are too weak in the ECMWF model and this is responsible for an underestimation of the downward sensible (upward latent) surface heat fluxes, leading to an
 348 additional overestimation of the SBL temperature and a subsequent too weak katabatic wind forcing. Note also that the surface slope is not well represented in ERA-15 because of its coarse horizontal resolution. Besides the resolution issue,
 351 simulated winds are also underestimated due to the first order turbulence closure schemes inside the ECMWF ERA-15 model (Gibson et al., 1999) that are known not to be adequate during stable conditions (Denby, 2001).

354

357 Table 3 : Statistics at ETH-Camp during the summer of 1991 based on 6-hourly values for the period from the 9th of May until the 30th of August.

Table 3

360 In addition to Figure 2 which shows daily average values during the whole
361 simulation period, Figure 3 demonstrates MAR ability to simulate correctly the
362 daily cycle for the most important near-surface atmospheric parameters during a
363 short period (June). The weather encountered during this month can be divided
364 into two distinct periods. Before the 16th of June, the weather was characterized
365 by a high-pressure synoptic situation that led to clear skies with large daily cycles
366 in temperature, humidity and wind speed. Afterwards, the surface pressure
367 dropped until the end of the month and clouds appeared which lead to damped
368 daily cycles of these atmospheric variables.

369

Figure 3

370 Figure 3: Comparison between observed (dotted) and MAR modelled (solid) air temperature, air
371 specific humidity, wind speed, wind direction, surface downward solar radiation and surface
372 downward longwave radiation at ETH-Camp from half-hourly values during June 1991.

373 The surface energy balance, which drives the surface mass balance, is largely
374 controlled by the radiative fluxes and the surface albedo and in a lesser extent by
375 the turbulent fluxes (van den Broeke et al., 1994). Table 4 contains the observed
376 averages, MAR bias and root mean square error for the radiative fluxes and this
377 for the whole duration of intensive radiative measurements at ETH-camp (June 3
378 until August 18), for cloudy days and for clear-sky days.

381

Table 4: Statistics of the radiative fluxes (in W m^{-2}) at ETH-Camp during the summer of 1991 (3
June - 18 August 1991) based on half hourly values.

384

Table 4

385 MAR overestimates the amount of incoming solar radiation. This overestimation
386 ($+ 26.5 \text{ W m}^{-2}$) is somewhat compensated by an underestimation (-14.7 W m^{-2}) of
387 the downward longwave radiation. Nevertheless, due to the high surface albedo
388 for snow (about 75 %), one has to conclude that the net radiation balance is still
389 underestimated by about 8 W m^{-2} .

Comparison between cloudy and clear sky conditions indicates that most of the

393 errors are caused during cloudy conditions. This is also shown in Figure 3 where
the largest errors in the simulated downward longwave radiation occur during
cloudy days, i.e. days with reduced solar downward radiation. In MAR, longwave
396 radiation is calculated with the scheme of Morcrette (1984) that was designed for
use in GCM models and that was also used during the calculation of the ERA-15
re-analysis. It was found by Morcrette (2002) that this version of the longwave
399 scheme underestimates the downward infrared radiation at the surface. In addition,
errors in the simulated cloud emissivities could further contribute to that negative
bias. This problem will be corrected in the future by using the new ECMWF
402 radiative transfer scheme (Morcrette, 2002).

405 During the 1991 ETH-expedition, eddy-correlation measurements were made to
evaluate the turbulent momentum and heat fluxes (Forrer and Rotach, 1997). Data
is only available during some periods of the ablation season. Therefore, we have
compared the model results with observations by means of scatter plots (Figure 4).

408

Figure 4

411 Figure 4: Comparison between simulated and observed 2m friction velocity (left) and sensible heat
flux (right) at ETH-Camp during the summer of 1991.

414 Simulated friction velocities are in agreement with the observations for values
lower than 0.3 m/s but show a positive bias at higher friction velocities. The
agreement is acceptable for the sensible heat flux at 2 m (negative values represent
downward heat fluxes) although MAR sometimes generates an upward sensible
417 heat flux, contrary to the observations. It is difficult to make definite conclusions
with only observations during some periods. Longer term continuous
measurements are needed given the uncertainty on eddy-correlation turbulent flux
420 measurements on sloping melting surfaces (Ohmura et al., 1992).

Figure 5

423 Figure 5: Top: Observed (dotted), MAR (solid) and ECMWF (dashed) cumulative precipitation at
ETH-Camp; Middle: same as above but for the surface albedo; below: same as top graph but for
the snow pack height.

426

The surface albedo variations, observed at ETH-Camp between the start of the

simulation and the end of July (Figure 5), are solely caused by snow grain metamorphism processes because the surface was covered with a sufficiently thick snow pack so that the underlying ice was not interfering. During this period, it can be seen (middle graph in Figure 5) that MAR modelled snow albedo closely follows the observed snow albedo variations, i.e. the lowering of the albedo due to growing snow grains when melt takes place and the abrupt increases due to snow falls simulated by the atmospheric model component. During these snow falls, fresh snow crystals with a high reflectance are deposited on top of the older larger snow grains. In particular, the timing of the onset and ending of the major melting period (3-26 July) coincides with the observations.

The disagreement at the beginning of August (01/08/1991 - 10/08/1991) is caused by the modelled ice layers at the surface of the snow pack. These ice layers with a low albedo of 0.55, form because of the lower air temperatures in combination with the saturated snow pack. It should be noticed that at the same moment, slush was observed in the surroundings of the site. This suggests that the slush is probably not well treated by the snow model during refreezing conditions.

Afterwards (11/08/1991 - 16/08/1991), due to the previously overamplified melt due to the underestimated surface albedo, the snow pack has become too thin in comparison with the observations. In these conditions, the model surface albedo is found to fluctuate between the high albedo coming from fresh snow and the low albedo (0.55) of the underlying ice. At the end of the simulation, simulated surface albedo values are again very close to the observations.

It should be stressed that a well simulated surface albedo is only possible provided all conditions are fulfilled. In particular, the surface albedo model should be sufficiently detailed but also the initial conditions should be correct. For example, the simulated height of the snow pack upon the ice at ETH-Camp decreases slightly too fast (lower graph in Figure 5) which causes the ice to appear to rapidly. This error can partly be explained by the somewhat underestimated mass balance of the initial snow pack caused by using a too small snow density at the beginning of the simulation (300 kg m^{-3}). Indeed the initial thickness of the snow pack is comparable to the observed one. This has been verified by comparison with the observed snow pack mass balance at ETH-Camp at the start of the simulation.

The use of a snow albedo which depends on the snow surface temperature in the ERA-15 re-analysis project clearly induces a too small albedo when melt occurs. It

can be seen that the ECMWF simulated surface albedo decreases down to 0.4
 465 already at the beginning of June. This oversimplified albedo scheme has been
 updated in the actual ECMWF forecast model as well as in the production of the
 new ERA-40 re-analysis dataset (personal communication A.Beljaars).

468

3.2. Model evaluation at the K-transect

During the GIMEX-91 experiment, 7 weather stations, 3 on the tundra and 4 on
 471 the ice sheet, were placed along the K(angerlussuq)-transect at 67 °N in west
 Greenland by the University of Utrecht and the Free University of Amsterdam.
 For more information about the experiment, the reader is referred to Van den
 474 Broeke et al. (1994), who give a detailed description of the measurement
 campaign. We will use data from only two stations (GIMEX-M6 and GIMEX-
 M9) which are both located on the ice sheet. MAR horizontal resolution (20 km)
 477 does not allow to compare model output with measurements from the other
 locations situated at 2.2 and 6.9 km from the ice sheet border. GIMEX-M6 and
 GIMEX-M9 are located at approximately 40 and 90 km from the ice sheet border
 480 (Table 2).

Figure 6

483 Figure 6: MAR (solid) and observed (dotted) air temperature, wind speed, wind direction, surface
 downward solar radiation and surface albedo evolution at GIMEX-M6.

486 Figures 6 and 7 compare MAR results with observations at GIMEX-M6 and
 GIMEX-M9, respectively. For GIMEX-M6, average hourly observations are
 available from 10 June until 24 July. At GIMEX-M9, half hourly observations for
 489 the 5-24 July period have been obtained. Unfortunately, no turbulent flux
 measurements by eddy-correlation were available for these GIMEX-sites.

492 Table 5: Statistics at GIMEX-M6 (hourly values) and GIMEX-M9 (half-hourly values) during the
 summer of 1991.

Table 5

495

Air temperature, air humidity, wind speed and wind direction are accurately
 simulated (Table 5). Solar downward radiation is overestimated which confirms

498 the results at ETH-Camp although the solar radiation evolution (Figure 6) shows
that the cloud cover frequency is mostly correctly simulated by the model.

501 The overestimated simulated surface albedo in MAR between 10th of June and
4th of July at GIMEX-M6 is due to the presence of an initial snow pack in the
504 MAR model. Actually, at the beginning of the measurements, the ice sheet surface
at GIMEX-M6 was snow-free. After the modelled snow pack in MAR has melted
away (4th July), the surface albedo agrees much better with the observed values.

507 **Figure 7**

Figure 7: as in Figure 6 but at GIMEX-M9. The dashed curves are from a sensitivity experiment in
which the surface albedo was held constant at 0.8 during the whole simulation and this over the
510 whole ice sheet.

At GIMEX-M9, the observed surface albedo between 5-24 July decreases from
513 0.8 to 0.65 (see Figure 7). Surface melt occurred on every day only interrupted by
one snowfall on July 16th. MAR modelled surface albedo also decreases due to
growing snow grains. However the modelled decrease is slightly too small.
516 Ablation at GIMEX-M9 is characterized by a strong daily cycle with melt during
the day and refreezing during the night (observed air temperatures fall below 0
° -C). This is successfully simulated by MAR.

519 The importance of an accurately simulated surface albedo clearly shows up when
the results of a sensitivity experiment are analyzed in which the surface albedo is
522 held constant at 0.8 over the whole sheet. This is shown for the GIMEX-M9
location (Figure 7) where the use of a constant albedo clearly leads to stronger
daily cycles because less heat from meltwater refreezing is available to act against
525 the cooling during the night. Moreover, a too high surface albedo tends to increase
the surface inversion, which increases the katabatic wind speed (visible between
22-27 July). But on average, the differences in the simulated atmospheric fields
528 between both experiments are rather small. This is also the case at GIMEX-M6
and ETH-Camp (not shown here).

However, there is a significant impact on the simulated mass balance (Table 6).
531 For example at GIMEX-M9 in the percolation zone, the initial snow height equals
141 cm above the ice. At the end of the simulation, this height is reduced to 61 cm
in the reference experiment while it is 50% higher (91 cm) in the albedo

534 sensitivity experiment. The impact is even larger at GIMEX-M6 situated in the
535 ablation zone characterized by low albedo values. At GIMEX-M6, the appearance
536 of ice at the surface is simulated on July 8th in the reference experiment with the
537 melt of an additional 130 cm of ice afterwards. At the end of the constant 0.8
538 albedo experiment, the winter snow pack at GIMEX-M6 is not even completely
539 melted away and 17 cm of snow remains above the ice at the end of August.

540

541 Table 6: Simulated surface mass balance components in the different model mass balance zones for
542 the reference experiment and the constant 0.8 albedo sensitivity experiment. The absolute mass
543 balance terms are expressed in mmWE. Negative numbers indicate mass losses. Net melt is the
544 amount of melt adjusted for retention of meltwater inside the snow pack and eventually refreezing.
545 The relative changes are calculated as $[(2) - (1)] / (1)$ with (1) the reference figures and (2) the
546 constant 0.8 albedo results.

Table 6

547 On average over the ice sheet (Table 6), melt decreases by more than 60% in the
548 constant albedo simulation compared to the reference experiment. The other mass
549 balance components only change in a minor way except the evaporative mass loss
550 which decreases by 10-15% in the model ablation and percolation zone.
551 Therefore, the use of a constant 0.8 albedo has little impact on the simulation of
552 the atmospheric variables but will lead to a significant underestimation of the
553 modelled melt. In the perspective of mass balance calculations, this is of capital
554 importance.

555 3.3. Model evaluation in the high dry snow zone (Summit)

556 AWS-Klinck is situated in the neighbourhood of the Greenland ice sheet summit.
557 The simulated temperature is in agreement with observations during the day but is
558 underestimated during the night when the temperature is below -25°C (Figure 8).
559 This leads to a negative temperature bias of about 3°C (Table 7). Part of the
560 negative bias can be explained by the katabatic temperature inversion and the
561 difference in height between the model's first level and the height of the
562 measurements. Indeed, the measurements were taken at a height of 3 m above the
563 surface while the model lowest level is situated at less than 1.5 m above the
564 surface. In fact, due to the elevated surface height of AWS-Klinck, the lowest

model level (pressure levels), which at mean sea level is normally situated at 2 m
570 above the surface is situated at 1.5 m above the surface near the summit of the
Greenland ice sheet. Secondly, as already explained during the discussion of the
573 results at ETH-Camp, Morcrette (2002) has shown that the radiative model used
in MAR (as well as in the ERA-15 re-analysis) underestimates the downward
infrared radiation for cold clear sky situations. This is responsible for an
underestimation of the air temperature, especially at the top of the ice sheet where
576 cold clear sky situations dominate. Again, the accuracy of the radiation physics in
polar conditions needs further improvement.

579 **Figure 8**

Figure 8: MAR (solid) and observed (dashed) air temperature, wind speed and surface pressure at AWS-Klinck which is located close to the ice sheet summit.

582 Table 7: Statistics at AWS-Klinck and Kangerlussuaq during the summer of 1991 based on 6-
hourly values.

585 **Table 7**

3.4. Model evaluation at Kangerlussuaq

588 At the start of the simulation, the tundra area near Kangerlussuaq is covered with
snow which explains why simulated air temperatures do not raise above 0 °C.
However, when all snow has melted away in the model, simulated temperatures
591 agree very well with the observed ones (Figure 9 and Table 7) stressing the need
for correct initial conditions for the simulation of the summer climate.
In this context, it also worth mentioning the results of Denby (2001) who found an
594 important sensitivity of the simulated turbulent and longwave heat fluxes in the
ice sheet ablation zone depending on the state of the tundra (snow covered or not).

597 **Figure 9**

Figure 9: MAR (solid) and observed (dotted) air temperature, relative humidity, wind speed,
surface pressure and cumulative precipitation at Kangerlussuaq.

600 The large surface pressure bias is caused by the difference in surface height (see

Table 2). The resolution used is clearly not yet sufficient to take explicitly into
603 account the narrow fjords which runs from the sea towards the ice sheet margins
through the tundra area.

606 Finally, MAR modelled precipitation corresponds closely with the observations
until half August (lower graph in Figure 9). Thereafter, about 4 precipitation
events are simulated by MAR at the right moment but with a too low intensity.
609 The precipitation bias can be due to very localised orographic effects in the
Kangerlussuaq fjord.

612

4. Conclusions and perspectives

615 A coupled atmosphere-snow regional climate model (MAR) applied over south
616 Greenland with a high horizontal resolution of 20 km has been nested into
617 ECMWF ERA-15 re-analysis. Lateral boundary conditions are updated every 6
618 hours. Due to the coupling of the regional climate atmospheric model with the
619 snow model, the snow albedo over the ice sheet is calculated by the snow model
620 from the precipitated fresh snow. Inside the snow model, the history of the
621 evolution of the snow grain characteristics (sphericity, dendricity and grain size) is
622 used to calculate the surface albedo.

618 The evaluation of the surface albedo simulation at ETH-Camp, GIMEX-M6 and
619 GIMEX-M9 showed that an accurate surface albedo simulation, which is a
620 requisite for a good surface mass balance simulation, strongly depends on the state
621 of the snow pack at the start of the ablation season. Therefore, future high-
622 resolution simulations of the Greenland surface mass balance by means of coupled
623 atmospheric-snow models should not only focus on the summer season but also on
624 the winter season. In that way, the initial conditions can be obtained more
625 accurately. Moreover close to the ice sheet margin around the K-transect, the ice
626 sheet surface is found to be snow-free at the start of the simulation. Winter
627 precipitation is not so important in this region (Bromwich et al., 2001a) but
628 certainly not equal to zero. On the other hand, the katabatic winds are very
629 persistent and strong in this region which suggests snow drift to take place. This,
630 as well as the role of evaporation and sublimation, should be further investigated
631 in the future.

618
621 Evaluation of the model surface radiative fluxes points to an overestimation of the
622 solar downward radiative flux and an underestimation of the longwave radiative
623 flux although the simulated inter-daily variability due to cloud cover was mostly
624 in agreement with the observations. The underestimation of the downward
625 longwave radiative flux with the present version of the longwave scheme has been
626 pointed out by Morcrette (2002) and will be corrected in the future by using an
627 updated version of the radiative scheme. Also the role of the microphysical
628 parameterizations should be further investigated.

621 A sensitivity experiment in which the surface albedo was held constant at 0.80
over the whole ice sheet underlined the strong influence of this parameter on the
simulation of the surface mass balance. This is particularly relevant in the model
624 ablation zone where ice appears at the surface during the summer melting season.
A constant 0.8 albedo influences weakly the atmospheric variables as in Cassano
et al. (2001). However on average over the ice sheet, there is 60% less melt. In the
627 perspective of mass balance calculations, it is therefore of capital importance to
use a variable albedo which evolves according to the state of the snow-ice surface.

624 The presented evaluation of the coupled atmosphere-snow Greenland climate
model opens new perspectives in the study of the Greenland surface mass balance
because of the coupling between the atmosphere and the snow model. In a next
step, the model should be applied over the whole Greenland ice sheet and
627 simulations covering longer time periods should be foreseen in order to study for
example, the origins and mechanisms behind the inter-annual variability of the
Greenland surface mass balance. Also sublimation and the contribution of
630 refreezing to the surface mass balance are topics that should be addressed with the
present model.

624

5. Acknowledgments

627 Filip Lefebre was financed by the Belgian Scientific Research Program "Global
Change and Sustainable Development (contract CG/10/09B)" of the Prime
Minister's Science Policy Office when writing this paper. We are very grateful to
the Belgian Royal Meteorological Institute (KMI-IRM) for opening the access to
630 the European Centre for Medium-Range Weather Forecasts (ECMWF) data
services. Dominique Lucas (ECMWF, Reading) is thanked for help with the ERA
data. The authors would like to thank The Antarctic Meteorological Research
633 Center, Space Science and Engineering Center, University of Wisconsin-Madison
a well as the National Science Foundation for the AWS-Klinck data. Philippe
Huybrechts (Vrije Universiteit Brussel, Brussels, Belgium) is kindly thanked for
636 providing the Greenland topography and land mask data. We gratefully
acknowledge the Belgian Fonds de la Recherche Fondamentale Collective, for
providing computer facilities under project 2.4556.99 "Simulation numérique et

627 traitement de données".

630 6. References

633 Ambach W (1988) Heat balance characteristics and ice ablation. western EGIG-profile, Greenland. In: Thomsen T, Søgaard H, Braithwaite R (eds) Applied hydrology in the development of northern basins, Danish Society for Arctic Technology, Copenhagen, pp 59-70

633 Benson CS (1962) Stratigraphic studies in the snow and firn of the Greenland ice sheet. SIPRE(CRREL) Res Rep 70, CRREL, Hannover NH, 93 pp

636 Brasseur O, Gallée H, Creutin J-D, Lebel T, Marbaix P (2002) High resolution simulations of precipitations over the Alps with the perspective of coupling with a hydrological model. In: Beniston M (eds) Climate Change: Implications for the hydrological cycle and for water management. Advances in Global Change Research, vol. 10, Kluwer Academic Publishers, Dordrecht (The Netherlands) and Boston (USA), pp 75-100

639 642 Box J, Steffen K (2001) Sublimation on the Greenland ice sheet from automated weather station observations, *J Geophys Res* 106: 33,965-33982

645 Bromwich D, Chen Q-S, Bai L, Cassano E, Li Y (2001a) Modeled precipitation variability over the Greenland ice sheet. *J Geophys Res* 106:33,891-33,908

648 Bromwich DH, Cassano JJ, Klein T, Heinemann G, Hines KM, Steffen K, Box JE (2001b) Mesoscale modeling of katabatic winds over Greenland with the Polar MM5. *Monthly Weather Review* 129(9): 2290-2309

651 654 Brun E, David P, Sudul M, Brunot G (1992) A numerical model to simulate snowcover stratigraphy for operational avalanche forecasting. *J Glaciol* 38:13-22

657 660 Cassano J, Box J, Bromwich D, Li L, Steffen K (2001) Evaluation of Polar MM5 simulations of Greenland's atmospheric circulation. *J Geophys Res* 106:33,867-33,890

663 Davies H (1983) Limitations of some common lateral boundary schemes used in regional NWP models. *Mon Wea Rev* 111:1002-1012

666 Deardorff J (1978) Efficient prediction of ground surface temperature and moisture with inclusion of a layer of vegetation. *J Geophys Res* 83:1889-1903

669 Denby B (2001) Modelling and interpretation of turbulent fluxes in katabatic flows: applications to glaciers and the Greenland ice sheet. PhD thesis, Universiteit Utrecht

666 669 Ekholm S (1996) A full coverage, high-resolution, topographic model of Greenland computed from a variety of digital elevation data. *J Geophys Res* 101(B10):21,961-21,972

672 Forrer J and Rotach W (1997) On the turbulence structure in the stable boundary layer over the Greenland ice sheet. *Bound-Layer Meteor* 85:111-136

672 Gallée H (1995) Simulation of the mesocyclonic activity in the Ross Sea, Antarctica. *Mon Wea Rev*

123:2051-2069

675

Gallée H and Duynkerke P (1997) Air-snow interactions and the surface energy and mass balance over the melting zone of West Greenland during GIMEX. *J Geophys Res* 102:13,813-13,824

678

Gallée H, Guyomarc'h G, Brun E (2001) Impact of snow drift on the Antarctic ice sheet surface mass balance: Possible sensitivity to snow-surface properties. *Bound-Layer Meteorology* 99 (1): 1-19

681

Gallée H and Schayes G (1994) Development of a three-dimensional meso- γ primitive equations model. *Mon Wea Rev* 122:671-685

684

Gallée H, Fontaine de Ghélin O, van den Broeke MR (1995) Simulation of atmospheric circulation during the GIMEX-91 experiment using a meso- γ primitive equations model. *J Climate* 8:2843-2859

687

Gibson JK, Kållberg P, Uppala S, Hernandez A, Nomura A, Serrano E (1999) ERA-15 Description (Version 2 – January 1999), ECMWF Re-analysis Project Report Series, European Centre for Medium-Range Weather Forecasts, Reading, UK

Georgi F, Mearns L (1999) Regional climate modeling revisited, *J Geophys Res* 104:6335-6352

693

Greuell W, Konzelmann T (1994) Numerical modelling of the energy balance and the englacial temperature of the Greenland ice sheet. Calculations for the ETH-Camp location (West Greenland, 1155 m a.s.l.). *Global Planet Change* 9:91-114

Hanna E, Valdes P (2001) Validation of ECMWF (re)analysis surface climate data, 1979-1998, for Greenland and implications for mass balance modelling of the ice sheet. *Int J Climatol* 21:171-195

Heinemann G (1999) The KABEG '97 field experiment: An aircraft-based study of katabatic wind dynamics over the Greenland ice sheet. *Bound-Layer Meteor* 93:75-116

Houghton J, Ding Y, Griggs D, Noguer M, van der Linden P, Dai X, Maskell K, Johnson C (eds) (2001) IPCC Climate Change 2001: The Scientific Basis. Contributions of Working Group I to the Third Assessment Report of the Intergovernmental Panel on Climate Change. Cambridge University Press, Cambridge, United Kingdom and New York, NY, USA, 881 pp

708

Huybrechts P, Letréguilly A, Reeh N (1991) The Greenland ice sheet and greenhouse warming. *Palaeogeogr Palaeoclim Palaeoecol* 89:399-412

711

Key J, Wang X, Stroeve J, Fowler C (2001) Estimating the cloudy sky albedo of sea ice and snow from space. *J Geophys Res* 106:12,489-12,497

714

Lefebre F, Gallée H, van Ypersele JP, Greuell W (2003) Modelling of snow and ice melt at ETH-Camp (west Greenland): a study of surface albedo. *J Geophys Res* 108(D8):4231 DOI:10.1029/2001JD001160

717

Marbaix P (2000) A regional atmospheric model over Europe: Adaptation for climate studies and validation. PhD thesis Université catholique de Louvain, Louvain-la-Neuve, Belgium

720

Marbaix P, Gallée H, Brasseur O, van Ypersele JP (2003) Lateral boundary conditions in regional climate

models: a detailed study of the relaxation procedure. *Mon Wea Rev* 131 (3):461-479

723

Morcrette J (1984) Sur la paramétrisation du rayonnement dans les modèles de la circulation générale atmosphérique. PhD thesis Univ. des Sciences et Techniques de Lille, Lille, France

726

Morcrette, J.-J. (2002) The surface downward longwave radiation in the ECMWF forecast system. *J. Climate* 15: 1875-1892.

729

Morris E, Bader H-P, Weilenmann P (1997) Modelling temperature variations in polar snow using DAISY. *J. Glaciology* 43(143): 180-191

732

Naithani J, Gallée H, Schayes G (2002) Marine air intrusion into the Adelie land sector of East Antarctica - A study using Regional Climate Model (MAR). *J Geophys Res* 107(D11) DOI:10.1029/2000JD000274

735

Nolin A, Stroeve J (1997) The changing albedo of the Greenland ice sheet: implications for climate modelling. *Ann Glaciol* 25: 51-57

738

Nomura A (1995) Global sea-ice concentration data set for use in the ECMWF re-analysis system. Technical Report 76, ECMWF, Shinfield Park, Reading

741

Oerlemans J, Vugts H (1993) A meteorological experiment in the melting zone of the Greenland Ice Sheet. *Bull Amer Meteor Soc* 74: 355-365

744

747

Ohmura A, Steffen K, Blatter H, Greuell W, Rotach M, Stober M, Konzelmann T, Forrer J, Abe-Ouchi A, Steiger D, Niederbäumer G (1992) Energy and mass balance during the melt season at the equilibrium line altitude, Paakitsoq, Greenland ice sheet: Progress report 2. Dep. of Geography, Swiss Federal Institute of Technology, Zürich

750

Ohmura A, Wild M, Bengtsson L (1996) A possible change in mass balance of Greenland and Antarctic ice sheets in the coming century. *J Climate* 9:2124-2135

753

Paterson W (1994) The physics of glaciers. Pergamon/Elsevier Science Ltd, 3rd ed

756

Pfeffer W, Meier M, Illangasekare T (1991) Retention of Greenland runoff by refreezing: implications for projected future sea level change. *J Geophys Res* 96:22,117-22,124

759

Reeh N (1991) Parameterization of melt rate and surface temperature on the Greenland ice sheet. *Polarforschung*, pp 113-128

762

Ritz C, Fabre A, Letréguilly A (1997) Sensitivity of a Greenland ice sheet model to ice flow and ablation parameters: consequences for the evolution through the last climatic cycle. *Climate Dyn* 13:11-24

765

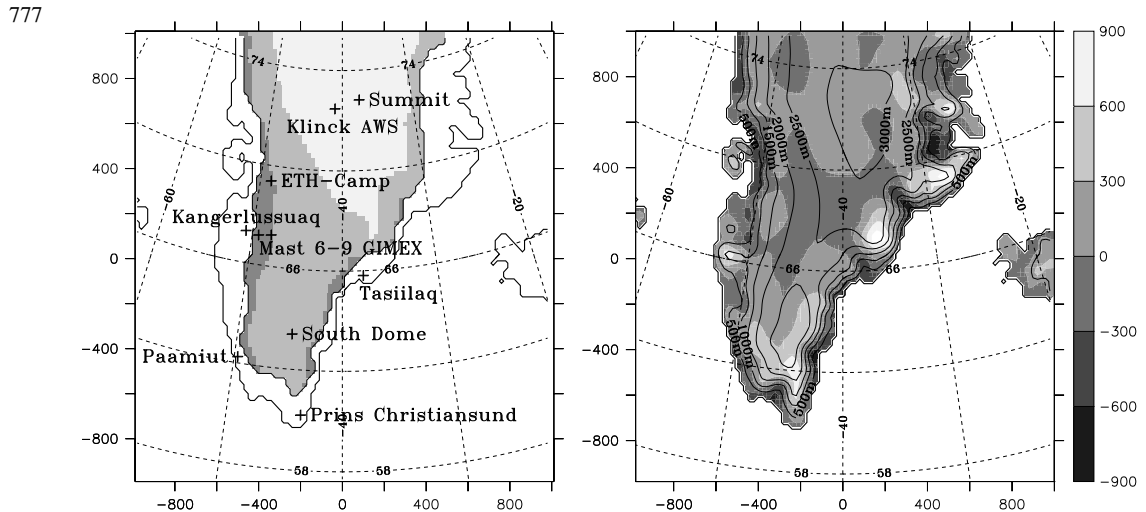
Schytt V (1958) The inner structure of the ice shelf at Maudheim as shown by core drilling. Norwegian-British-Swedish Antarctic Expedition, 1949-52, Scientific Results 4, Glaciology 2, Norsk Polarinstitutt, Oslo, pp 115-151

768

Thomas RH, PARCA Investigators (2001) Program for arctic regional climate assessment (PARCA): Goals, key findings, and future directions. *J Geophys Res* 106(D24): 33691-33705

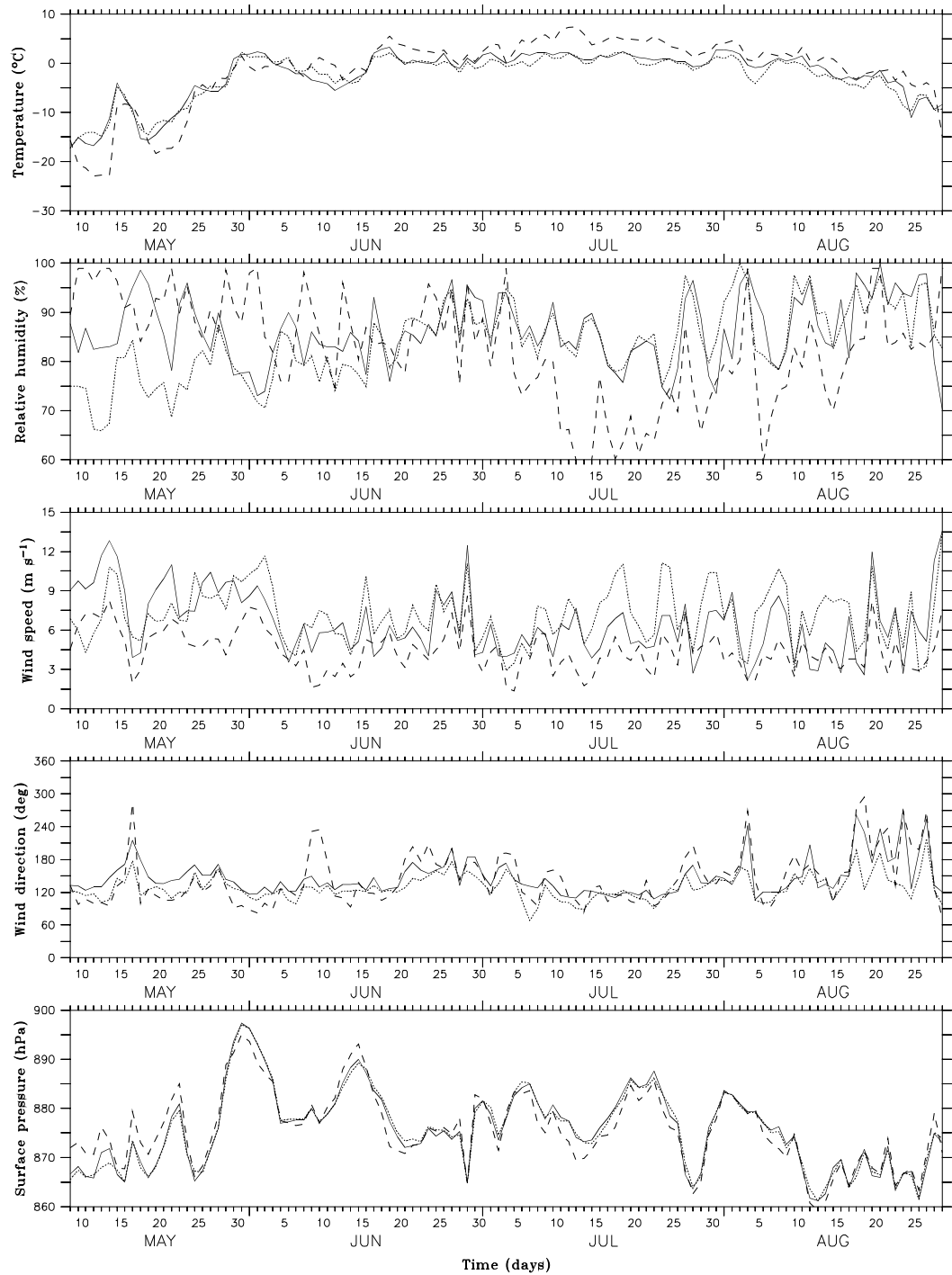
771 van de Wal R, Oerlemans J (1994) An energy balance model for the Greenland ice sheet. *Global Planet Change* 9:115-131

774 van den Broeke MR, Duynkerke P, Oerlemans J (1994) The observed katabatic flow at the edge of the Greenland ice sheet during GIMEX-91. *Global Planet Change* 9:3-15



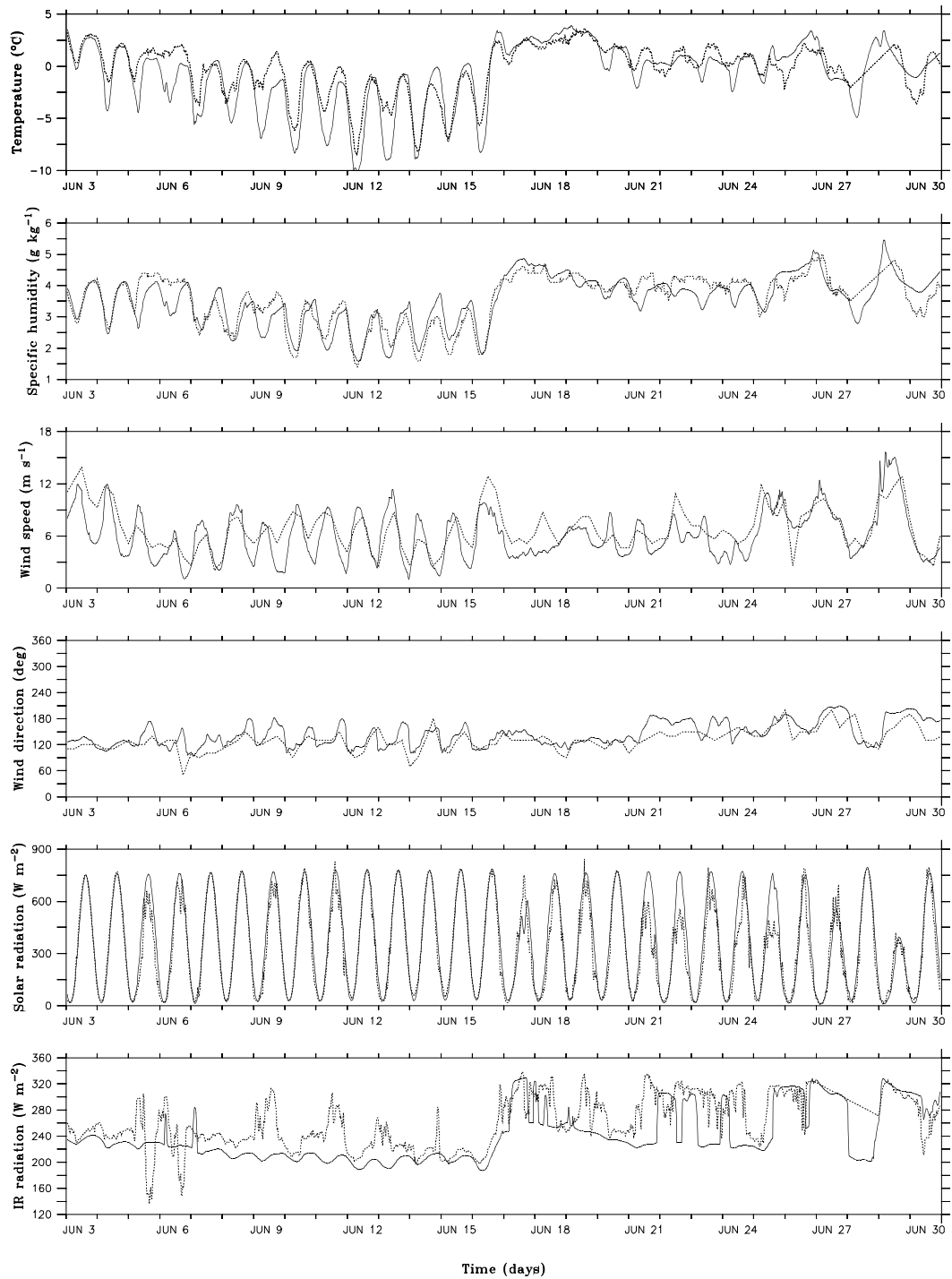
780 Figure 1: The prescribed distribution of MAR mass balance zones on the Greenland ice sheet and
 781 the major locations referred to in the text. From black to light grey over the ice sheet: ice sheet
 782 ablation zone, percolation zone and dry snow zone. The model ablation zone delineation is
 783 specified and taken from Reeh (1991). (Right) MAR surface height (isolines) and the difference
 784 (shades of grey) between MAR and ECMWF model surface height.

780



783 Figure 2: Comparison between observed (dotted), MAR (solid) and ECMWF (dashed) modelled
 air temperature, relative humidity, wind speed, wind direction and surface pressure (daily average
 values) at ETH-Camp during the whole simulation.

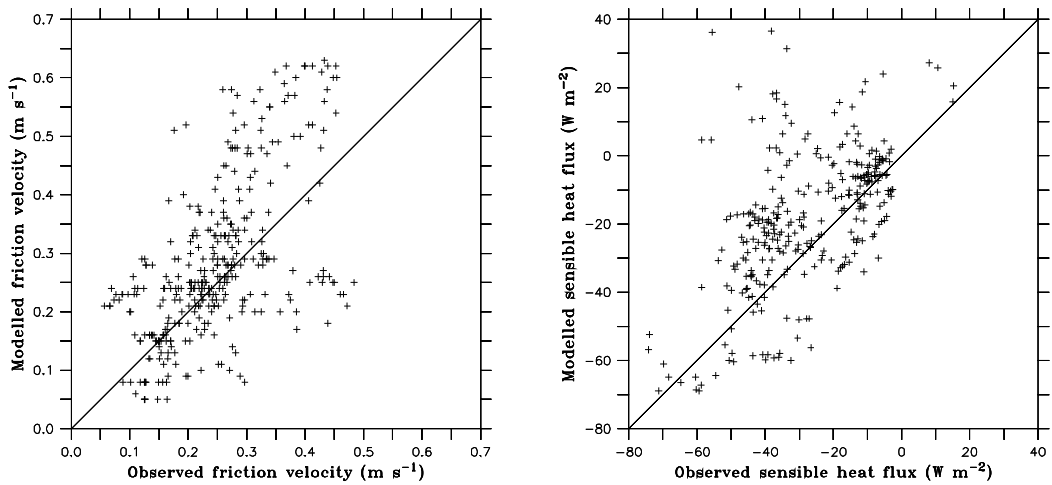
786



789 Figure 3: Comparison between observed (dotted) and MAR modelled (solid) air temperature, air
 790 specific humidity, wind speed, wind direction, surface downward solar radiation and surface
 791 downward longwave radiation at ETH-Camp from half-hourly values during June 1991.

792

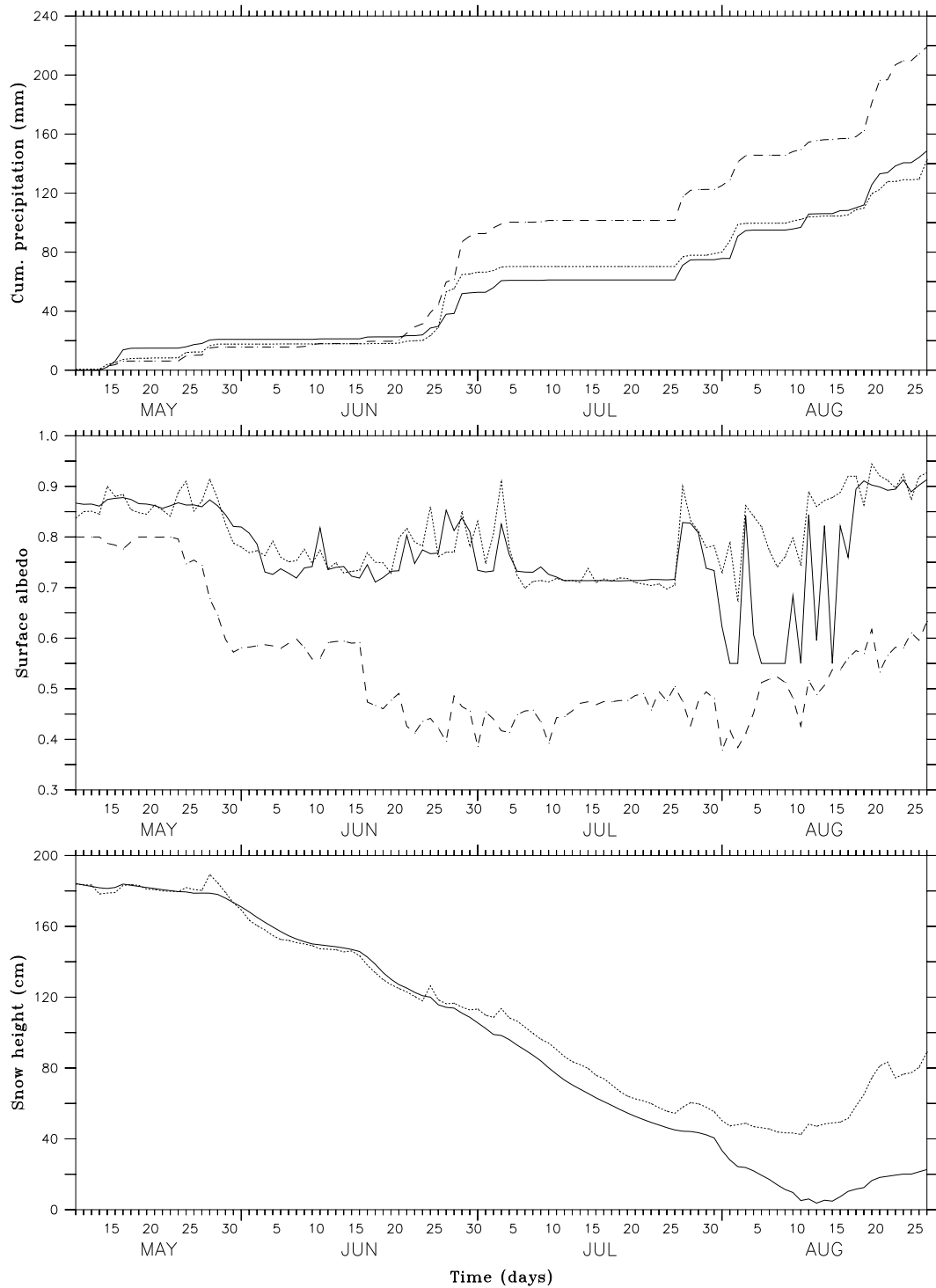
795



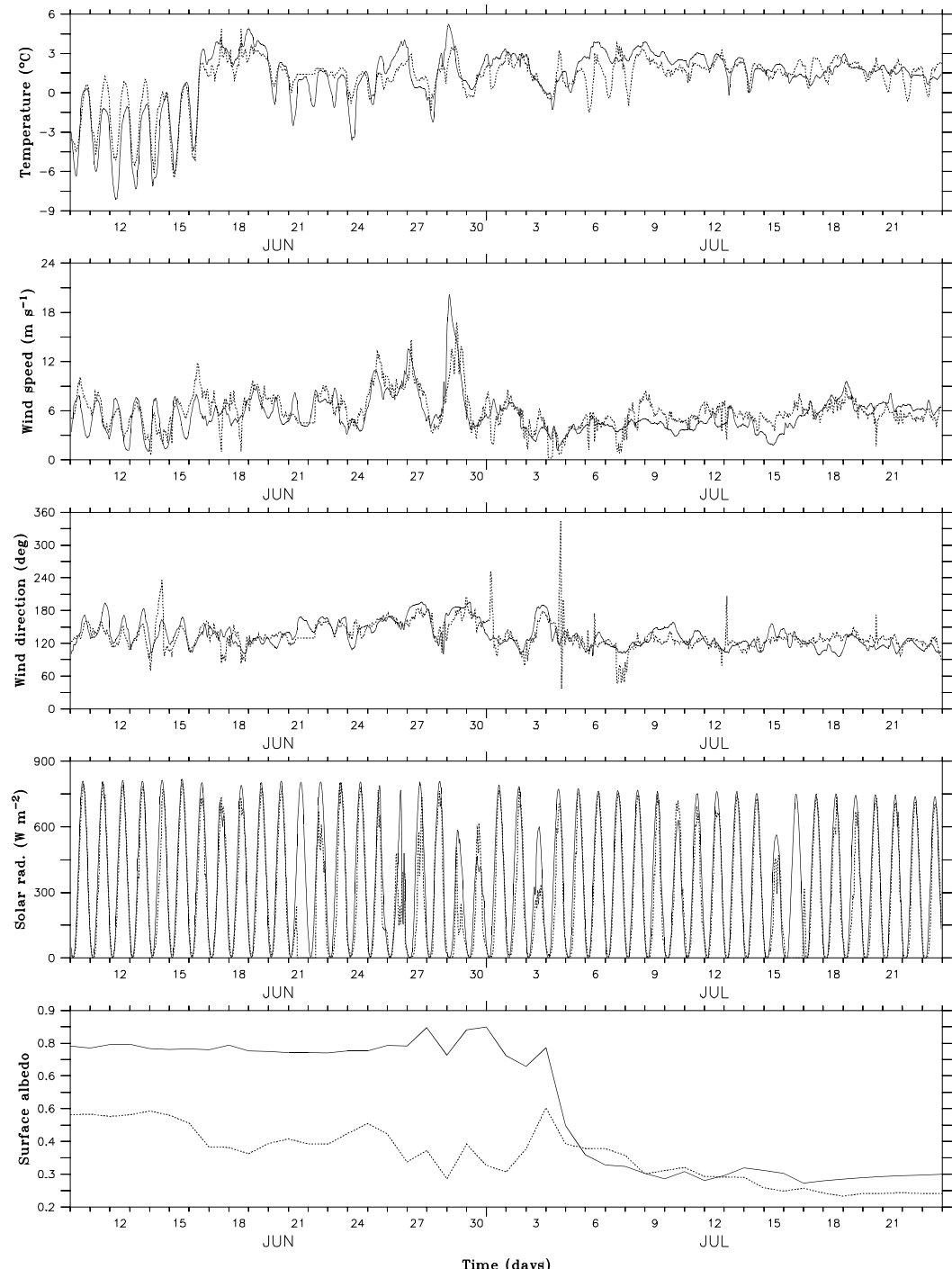
798

Figure 4: Comparison between simulated and observed 2m friction velocity (left) and sensible heat flux (right) at ETH-Camp during the summer of 1991.

801



804 Figure 5: Top: Observed (dotted), MAR (solid) and ECMWF (dashed) cumulative precipitation at
 ETH-Camp; Middle: same as above but for the surface albedo; below: same as top graph but for
 the snow pack height.



807

Figure 6: MAR (solid) and observed (dotted) air temperature, wind speed, wind direction, surface downward solar radiation and surface albedo evolution at GIMEX-M6.

810

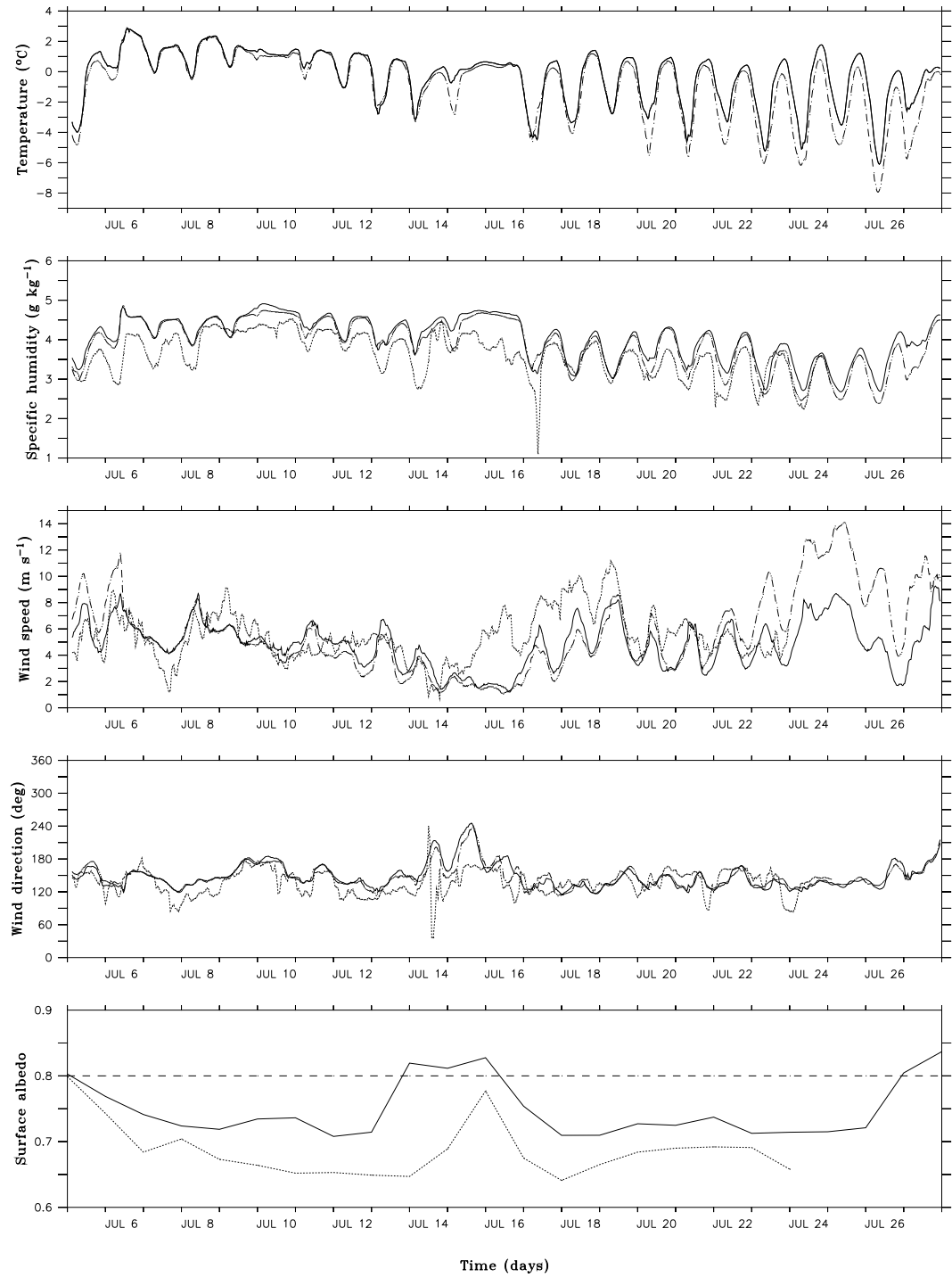
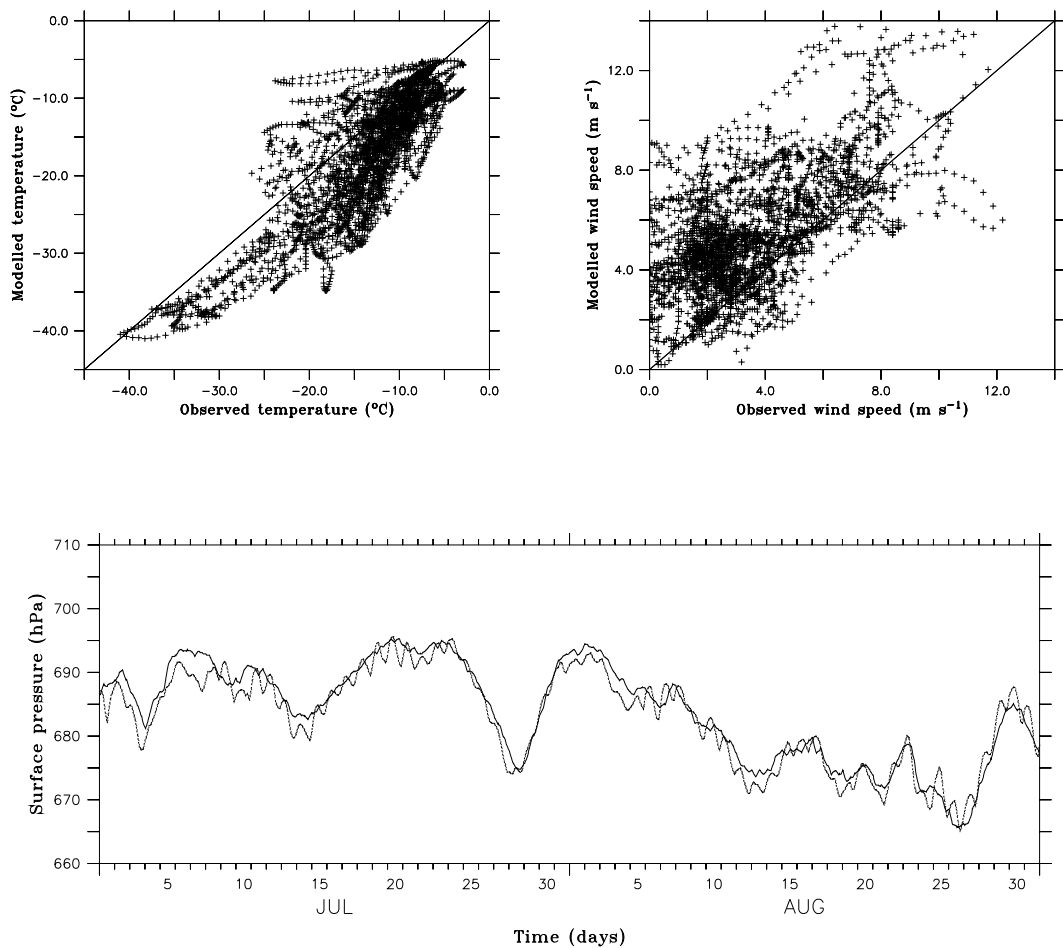


Figure 7: as in Figure 6 but at GIMEX-M9. The dashed curves are from a sensitivity experiment in
 813 which the surface albedo was held constant at 0.8 during the whole simulation and this over the
 whole ice sheet.

813



816 Figure 8: MAR (solid) and observed (dashed) air temperature, wind speed and surface pressure at AWS-Klinck which is located close to the ice sheet summit.

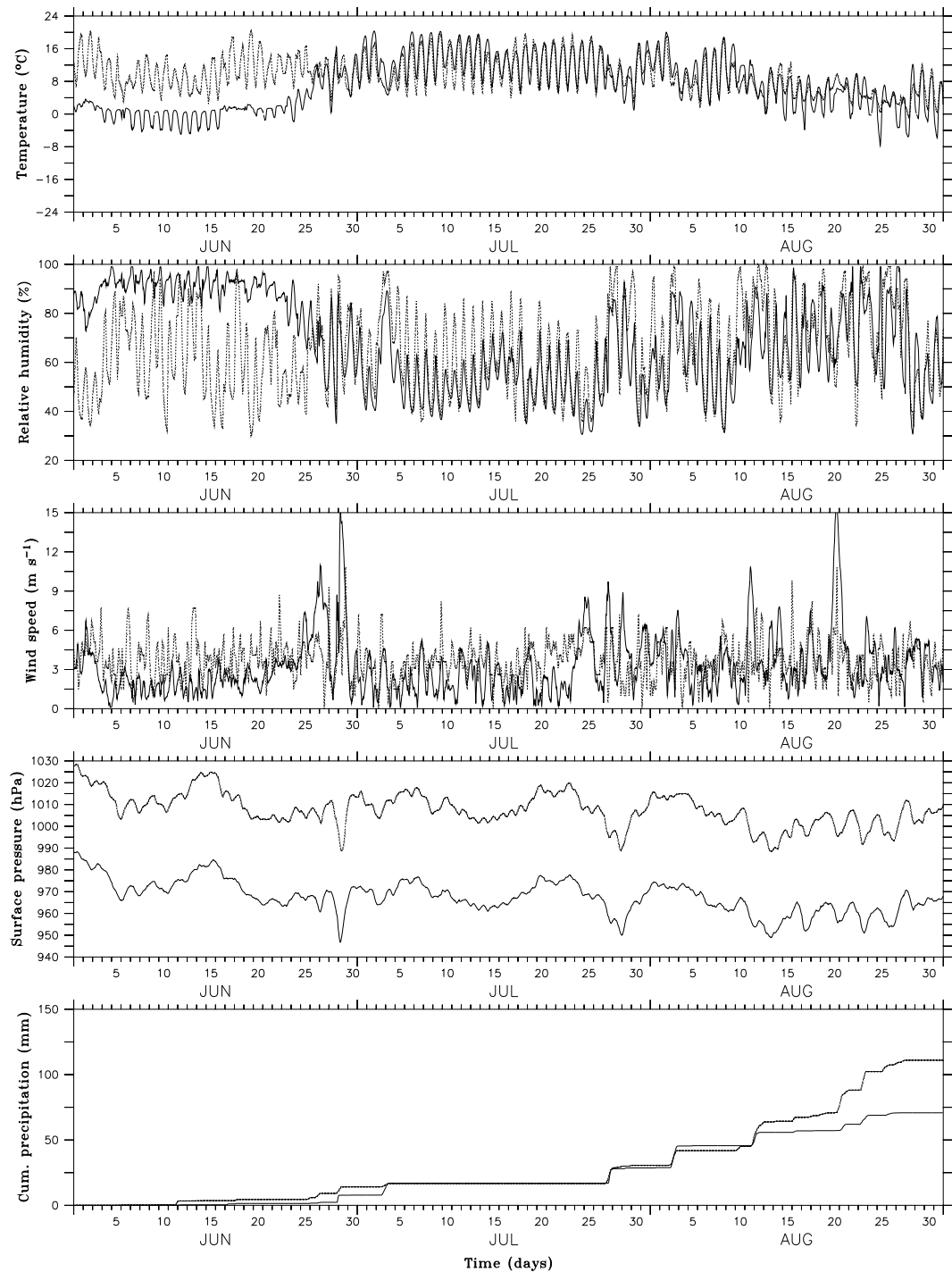


Figure 9: MAR (solid) and observed (dotted) air temperature, relative humidity, wind speed, surface pressure and cumulative precipitation at Kangerlussuaq.

Table 1: Snow-ice model initial state characteristics.

Model mass balance zone	Vertical structure	Snow-ice model density (kg m ⁻³)	Snow grain size (mm)
Dry snow zone	20 m of snow	eq. 2	0.3
Percolation zone	20 m of snow	500	0.3
	+		
	Bromwich (2001a) 1990-1991 winter snow	300	0.3
Ablation zone	20 m ice	920	-
	+	+	
	Bromwich (2001a) 1990-1991 winter snow	300	0.3
Tundra area	Bromwich (2001a) 1990-1991 winter snow	300	0.3

825 Table 2: Geographical positions and elevations of the locations used in the comparison.

Site	Latitude (°N)	Longitude (°W)	Observed Elevation	MAR elevation	ERA elevation
ETH-Camp	69.57	49.29	1155	1153	1266
GIMEX-M6	67.06	49.35	1028	1027	1143
GIMEX-M9	67.03	48.28	1520	1597	1607
AWS-Klinck	72.31	40.48	3105	3080	3019
Kangerlussuaq	67.01	50.70	50	340	692

828 Table 3 : Statistics at ETH-Camp during the summer of 1991 based on 6-hourly values for the
 period from the 9th of May until the 30th of August.

Variable	Obs. mean	MAR bias	ERA bias	MAR rmse	ERA rmse	MAR corr	ERA corr
Air temperature (°C)	-2.77	+0.39	+1.42	1.99	4.16	0.94	0.86
Relative humidity (%)	83.86	+1.58	-2.12	7.43	14.98	0.63	0.01
Wind speed (m s ⁻¹)	7.17	-0.60	-2.70	2.70	3.56	0.60	0.54
Wind direction (°)	128.6	+18.0	+16.5	35.4	50.0	0.66	0.59
Surface pressure (hPa)	875.8	-0.04	+0.00	1.21	2.69	0.99	0.94
Surface albedo (-)	0.75	-0.05	-0.25	0.11	0.26	0.53	0.49

831 Table 4: Statistics of the radiative fluxes (in W m^{-2}) at ETH-Camp during the summer of 1991
 (3 June - 18 August 1991) based on half hourly values.

Period	Variable	Observed mean	MAR bias	MAR rmse	MAR corr
3 rd June ↔ 18 th August	Solar ↓	301.11	+26.46	78.11	0.96
	IR ↓	261.51	-14.68	34.51	0.62
Cloudy	Solar ↓	222.79	+53.83	117.35	0.92
	IR ↓	302.81	-22.68	47.56	0.27
Clear Sky	Solar ↓	340.11	+9.60	47.76	0.98
	IR ↓	240.95	-10.95	25.63	0.42

834 Table 5: Statistics at GIMEX-M6 (hourly values) and GIMEX-M9 (half-hourly values) during the summer of 1991.

Station	Variable	Obs mean	MAR bias	MAR rmse	MAR corr
GIMEX-M6 (10-24 July)	Air temperature (°C)	1.08	+0.07	1.18	0.86
	Wind speed (m s ⁻¹)	6.00	-0.37	1.76	0.72
	Wind direction (°)	133.40	-1.18	20.75	0.61
	Solar ↓ rad. (W m ⁻²)	304.30	+44.37	99.50	0.95
	Surface albedo (-)	0.40	+0.16	0.21	0.76
GIMEX-M9 (5-24 July)	Air temperature (°C)	-0.34	+0.25	1.16	0.79
	Air spec hum. (g kg ⁻¹)	3.61	+0.47	0.56	0.83
	Wind speed (m s ⁻¹)	5.643	-0.87	1.99	0.55
	Wind direction (°)	136.2	+11.72	27.52	0.40
	Surface albedo (-)	0.69	+0.05	0.07	0.62

837

840 Table 6: Simulated surface mass balance components in the different model mass balance zones for
 841 the reference experiment and the constant 0.8 albedo sensitivity experiment. The absolute mass
 842 balance terms are expressed in mmWE. Negative numbers indicate mass losses. Net melt is the
 843 amount of melt adjusted for retention of meltwater inside the snow pack and eventually refreezing.
 The relative changes are calculated as $[(2) - (1)] / (1)$ with (1) the reference figures and (2) the
 constant 0.8 albedo results.

Area	Variable	Reference experiment	Albedo sens. experiment	Relative change (%)
Ablation zone	Mass balance change	-703.6	-109.6	-84.42
	Net melt	-958.4	-365.1	-62.91
	Sublimation	-26.7	-22.8	-14.61
	Rainfall	112.9	106.7	-5.49
	Snowfall	168.6	171.6	-1.78
Percolation zone	Mass balance change	272.4	270.9	-0.55
	Net melt	-5.0	-4.5	-10.00
	Sublimation	-24.9	-22.4	-10.04
	Rainfall	21.7	20.9	-3.69
	Snowfall	280.6	276.9	-1.32
Dry snow zone	Mass balance change	130.12	127.22	-2.23
	Net melt	0.00	0.00	0.00
	Sublimation	-10.00	-9.60	-4.00
	Rainfall	1.72	1.68	-2.33
	Snowfall	138.40	135.10	-2.38
Whole ice sheet	Mass balance change	121.5	176.1	44.94
	Net melt	-93.5	-37.0	-60.43
	Sublimation	-19.2	-17.2	-10.42
	Rainfall	22.2	21.2	-4.50
	Snowfall	212.0	209.1	-1.37

846

849

852

Table 7: Statistics at AWS-Klinck and Kangerlussuaq during the summer of 1991 based on 6-hourly values. The large MAR surface pressure bias and rmse at Kangerlussuaq is caused by the 290 m difference in surface height (Table 2).

Station	Variable	Obs mean	MAR bias	MAR rmse	MAR corr
AWS-Klinck (1 st May ↔ 31 st August)	Air temperature (°C)	-15.66	-3.12	5.12	0.87
	Wind speed (m s ⁻¹)	4.08	+1.8	2.64	0.72
	Wind direction (°)	164.8	+12.87	55.73	0.62
	Surface pressure (hPa)	683.10	+0.91	1.98	0.98
Kangerlussuaq (1 st May ↔ 31 st August)	Air temperature (°C)	7.52	-4.74	7.08	0.78
	Relative humidity (%)	65.13	+11.06	23.80	0.30
	Wind speed (m s ⁻¹)	3.64	-0.82	2.27	0.19
	Surface pressure (hPa)	1008.0	-40.48	40.36	0.98

855